P1.6 AEROSOL RADIATIVE FORCING ESTIMATED FROM GROUND-BASED RADIATION MEASUREMENTS AT GAME/AAN SITES

Dohyeong Kim[1], B. J. Sohn[1], T. Nakajima[2], I. Okada[3], T. Takamura[3]
School of Earth and Environmental Sciences, Seoul National University[1],
Center for Climate System Research, University of Tokyo[2],
Center for Environmental Remote Sensing, Chiba University[3]

1. INTRODUCTION

It has been well known that aerosols can give profound impact on global and regional climates, both directly by interfering with solar radiation and indirectly by modifying cloud microphysics associated with CCN (cloud condensation nuclei) or IC (ice nuclei) changes. Global average of annual radiative forcing by anthropogenic aerosols ranges from about –0.3 to –2 W m^{-2} that is comparable to the forcing induced by greenhouse gas increases during the last century (Charlson et al., 1992; Kiehl and Briegleb, 1993). However, it is noted that those values are subject to a great deal of uncertainty by more than a factor of two (Schwartz, 1996). Recent model estimates showed that the inclusion of absorbing aerosols such as black carbon in climate model can even change the sign of aerosol forcing from negative to positive (Liao et al., 1998; Haywood et al., 1998), reflecting the uncertainties in radiative forcing estimation. The role of aerosols in climate has not been completely understood and thus it is very important to reduce uncertainties in determining aerosol characteristics for examining the role of aerosol in climate changes.

Because of importance of aerosols in the climate change studies, field experiments are much needed to reduce those uncertainties. Several field experiments such as Aerosol Characterization Experiment [ACE1 and ACE2], Tropospheric Aerosol Radiative Forcing Observational Experiment [TARFOX] (Russell et al., 1999) and Indian Ocean Experiment [INDOEX] (Ramanathan et al., 1996) were taken places to observe the optical and chemical properties of aerosols which can be used for parameterizations for climate model. In line with those field experiments, Aerosol Robotic Network [AERONET] also collects the aerosol optical properties based on the world-wide ground-based aerosol monitoring network consisting of automatic sun-sky scanning spectral radiometers.

On the other hand, as a part of the GAME/AAN (GEWEX Asian Monsoon Experiment/ Asian AWS Network) a ground-based aerosol/radiation observation network named as the SKYNET was established. In order to study the role of aerosol in climate over the Asian continent, sky radiance data as well as solar radiative fluxes are measured at the SKYNET observation sites. The primary objective of the SKYNET is to estimate direct and indirect radiative forcings of aerosols on climatological time and space scales. In determining the forcing over the Asian continent, we calculate downward radiative fluxes at the surface using a radiative transfer model in which optical properties derived from SKYNET observations are used as inputs. Radiation fluxes at the top of the atmosphere (TOA) are also calculated by matching the calculated surface radiation flux to measured values.

2. SURFACE MEASUREMENTS OF SOLAR RADIATION

The solar radiation data at GAME/AAN sites of Sri-Samrong (17.17°N, 99.87°E) in Thailand and Mandalgovi (45.59°N, 106.19°E), Dunhuang (40.16°N, 94.80°E), Hefei (31.90°N, 117.16°E), Shouxian (32.55°N, 116.78°E), Yinchuan (38.48°N, 106.22°E) in China measured from 1998 to 2000, are analyzed in order to characterize the regional background aerosol optical properties and their effect on the surface radiation budget. Also analyzed are data collected from surface solar radiation sites at Anmyon-Do (36.52°N, 126.32°E) of Korea and Amami-Oshima (28.44°N, 129.70°E) in Japan where the measured solar radiations reflect more of aerosol characteristics in coastal and marine environments, and thus we can examine the aerosol influences on surface solar radiation under such environments.

2.1 Sky radiometer data

Measurements of direct and diffuse solar radiation are taken with the sky radiometer (POM-01L) at the wavelength of 315, 400, 500, 675, 870, 940, and 1020 nm. The aerosol optical thickness, size distribution, single-scattering albedo, and complex refractive index were derived by using the SKYRAD.pack retrieval software, which consists of a radiative transfer code as well as linear and nonlinear inversion scheme (Nakajima et al., 1996b). The aerosol optical thickness, $\tau_a(\lambda)$, is defined as:

$$\tau_a(\lambda) = \int_{rm}^{rM} \pi r^2 Q_{ext}(x, m) n(r) dr \qquad (1)$$

where Q_{ext} is the efficiency factor for extinction as given by Mie theory for spherical particles, $x=(2\pi/\lambda)r$ is size parameter, $n(r)$ is columnar radius distribution of aerosol, r_m and r_M are minimum and maximum aerosol radii, respectively, and $m=m_r - im_i$ is aerosol complex refractive index.

2.2 Solar radiative flux data

Pyranometer is used for measuring total downward solar fluxes and diffused solar radiative fluxes by solar occultation method in the wavelength region between 0.3 and 2.8 μm to avoid the emission for longer wavelength. Direct solar fluxes are estimated by the pyheliometer which measures the intensity of a radiant beam at normal incidence coming only from the solar disk in about 5 degree of

circumsolar radiation.

3. RESULTS

3.1 Analyses of the sky radiometer data

In order to examine the optical characteristics as a wavelength dependence of optical thickness we present the Ångström exponent α

$$\tau_{a\lambda} = \tau_{0.5}\left(\frac{\lambda}{0.5}\right)^{-\alpha} \quad (2)$$

where λ's are wavelengths. We show the scatterplot of $\tau_{0.5}$ versus α in Fig. 1. Since Ångström exponent (α) represents characteristics of basic properties of aerosols more efficiently, the contrasting difference between mean α's (1.028 vs 0.205 at Sri-Samrong and Dunhuang, respectively) strongly suggests that the main component of particles is composed of sub-micron particles in Sri-Samrong whereas sand-dust like particles in Dunhuang. It is noted that most Chinese stations show a negative correlation between $\tau_{0.5}$ and α, especially in spring. These findings are in good agreement with results from Nakajima et al. (1989) that a negative correlation can be explained by growing aerosol particles associated with soil-derived particles whose characteristic α is close to 0. These are also consistent with Kaufman et al. (1994) that the desert transition zone has a negative correlation. In Anmyon-Do, located at the Korean coastal region, various sizes of aerosol particles are found as seen in α ranging from 0.2 to 2.0. We can clearly see the features of Asian dust with small α and large $\tau_{0.5}$ at both Anmyon and Amami-Oshima, Japanese island.

3.2 Simulation of surface solar radiative flux

Surface solar radiative fluxes are integrated over wavelengths from 0.3 to 2.8 μm using the radiative transfer model (rstar5b) developed by Nakajima et al. (1988). For the calculation we used the measured aerosol optical properties derived from sky radiation measurements at GAME/AAN sites. Retrieved aerosol optical properties, such as aerosol optical thickness, size distribution, are used for describing the atmospheric aerosol under clear sky condition. For the simulation under cloudy sky condition, we used cloud fraction and cloud optical thickness, which are retrieved from GMS-5 measurements (Okada et al., 2000). Random cloud overlapping is applied for the vertical distribution of clouds. For the atmospheric profiles, we used 6-hourly NCEP (National Centers for Environmental Prediction) reanalysis data and total ozone amounts from TOMS (Total Ozone Mapping Spectrometer) are used for calculating ozone absorption.

Fig. 2(a) shows simulation results under clear sky condition, which was determined by examining time series of surface measured solar radiative fluxes for a given local time in interest. The comparison between estimated and measured fluxes at Mandalgovi in 1998 shows a good agreement within 10 W m^{-2}. The diffuse fluxes at Sri-Samrong in March show overestimation of the simulated solar fluxes than surface measured fluxes, but in December 1998, the simulated solar fluxes show underestimates. The discrepancy is likely due to inaccurate input parameters such as water vapor amount, aerosol absorption index (absolute value of imaginary part of the aerosol refractive index), and aerosol vertical structure under clear sky condition. Furthermore, surface fluxes much depend on the loadings of atmospheric gases and aerosols even at one fixed station. Considering the fact that atmospheric conditions in the high-latitude dry area are less variant in comparison with low-latitude moist Sri-Samrong area, the more agreement found in Madalgovi manifests the impact of input parameters on uncertainties in derived surface radiation budget. More accurate retrievals of aerosol optical characteristics should reduce the differences between simulated and measured solar fluxes.

Fig. 2(b) shows simulation results under the cloudy sky condition, which was determined by using GMS-5 cloud fraction and cloud optical thickness. For sky radiometer is not available in cloudy sky condition, we should use the aerosol optical properties via time interpolation. The results at Mandalgovi show overestimates in lower flux sides. By contrast, simulated results in Sri-Samrong show overestimates if measured values are located between 100 and 200 W m^{-2}, which represents underestimation of cloud optical thickness from GMS-5 image data.

The rms (root mean square) errors of Mandalgovi and Sri-Samrong are 6.3 and 9.7 W m^{-2} under the clear sky condition, 36.6 and 42.9 W m^{-2} under the cloudy sky condition, respectively. For simulation of surface solar radiation under the cloudy sky condition, more accurate retrieval of cloud optical thickness should be needed.

3.3 Aerosol radiative forcing

Aerosol radiative forcing was calculated using the measured aerosol optical properties derived from sky radiation measurements at GAME/AAN sites in conjunction with a radiative transfer model. In order to avoid the dependence on solar zenith angle in aerosol radiative forcing calculation, we use 24-hour averaged radiative forcing. In the calculations, constant aerosol optical thickness is assumed throughout the day.

Fig. 3 shows instantaneous aerosol radiative forcing per unit optical thickness at 0.5 μm as a function of local standard time at the surface and TOA. The difference among the stations and seasons appear to be due primarily to the differences in particle size distribution, wavelength dependence of optical thickness and absorption index. Some of the differences may be induced by aerosol optical thickness, because the aerosol radiative forcing is not exactly a linear function of aerosol optical thickness (Russell et al., 1997).

Fig. 4 presents aerosol radiative forcing averaged over the 24-hour period for a given aerosol

optical thickness at 0.5 μm. The results show that downward fluxes are varied with aeorosol changes in the range of -30 to -110 W m^{-2} per unit aerosol optical thickness at the surface. The different magnitudes of aerosol radiative forcing are likely due to the aerosol characteristics depending on different geographic locations. The smaller values at Sri-Samrong in Thailand result from decreasing forward peaking of the scattering by a smaller aerosol effective radius, consistent with TARFOX results (Russell, 1999).

4. ACKNOWLEDGMENTS

This research has been supported by the CES funded through KOSEF.

5. REFERENCES

Charlson, R. J., S. E. Schwartz, J. M. Hales, R. D. Cess, J. A. Coakley Jr., J. E. Hansen, and D. J. Hofmann, 1992: Climate forcing by anthropogenic aerosols. *Science*, 255, 423-430.

Haywood, J. M., and V. Ramaswamy, 1998: Global sensitivity studies of the direct radiative forcing due to anthropogenic sulfate and black carbon aerosols. *J. Geophys. Res*., 103, 6043-6058.

Kaufman, Y. J., A. Gitelson, A. Karnieli, E. Ganor, R. S. Fraser, T. Nakajima, S. Mattoo, and B. N. Holben, 1994: *J. Geophys. Res*., 99, 10341-10356.

Kiehl, J. T., and B. P. Briegleb, 1993: The relative roles of sulfate aerosols and greenhouse gases in climate forcing. *Science*, 260, 311-314.

Liao, H., and J. H. Seinfeld, 1998: Effect of clouds on direct aerosol radiative forcing of climate. *J. Geophys. Res*., 103, 3781-3788.

Nakajima, T and T. Nakajima, 1995: Wide-area determination of cloud microphysical properties from NOAA AVHRR measurements for FIRE and ASTEX regions. *J.A.S*., 52, 4043-4059.

Nakajima, T and M. Tanaka, 1988: Algorithms for radiative intensity calculations in moderately thick atmospheres using a truncation approximation, *J. Quant. Spectrosc. Radiat. Transfer*, 40, 51-69.

Nakajima, T., G. Tonna, R. Rao, R. Boi, Y. Kaufman, and B. Holben, 1996b: Use of sky brightness measurements from ground for remote sensing of particulate polydispersions, *Applied Optics*, 35, 2672-2686.

Nakajima, T. and A. Higurashi, 1997: AVHRR remote sensing of aerosol optical properties in the Persian Gulf region, summer 1991. *J. Geophys. Res*., 102, 16935-16946.

Okada, I., T. Takamura, K. Kawamoto, T. Inoue, Y. Takayabu, and T. Kikuchi, 2000: Cloud cover and optical thickness from GMS-5 image data. *Proc. GAME AAN/Radiation Workshop*, Phuket, 8-10 March, 2001, 9-11.

Russell, P. B., J. M. Livingston, P. Hignett, S. Kinne, J. Wong, A. Chien, R. Bergstrom, O. Durkee, and P. V. Hobbs, 1999: Aerosol-induced radiative flux changes off the United States mid-Atlantic coast: Comparison of values calculated from sunphometer and in situ data with those measured by airborne Pyranometer. *J. Geophs. Res*. 104, 2289-2307.

Schwartz, S. E., 1996: The whitehouse effect – shortwave radiative forcing of climate by anthropogenic aerosols: An overview. *J. Aerosol Sci*., 27, 359-382.

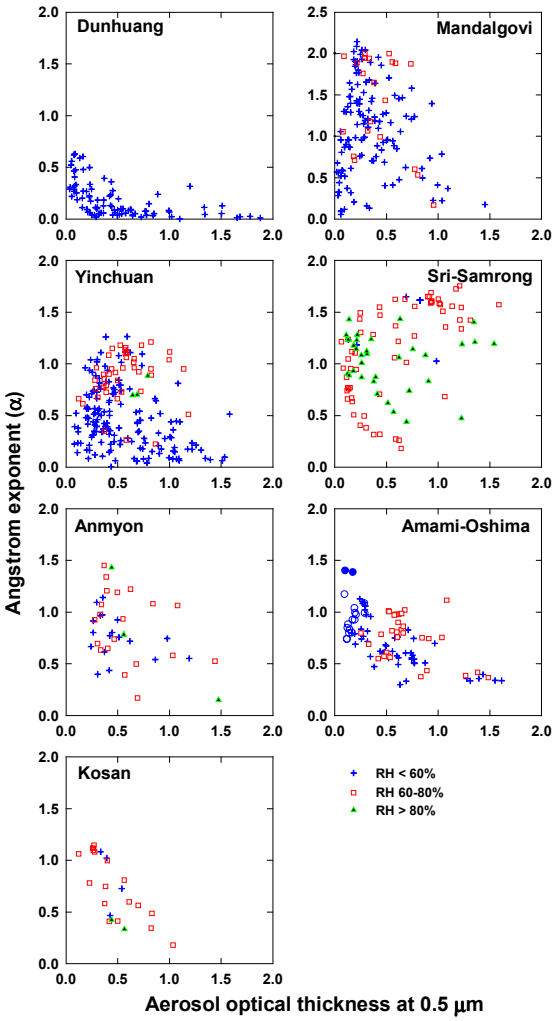

Fig. 1: Scatterplot of the Ångström exponent versus aerosol optical thickness at the wavelength of 0.5 μm.

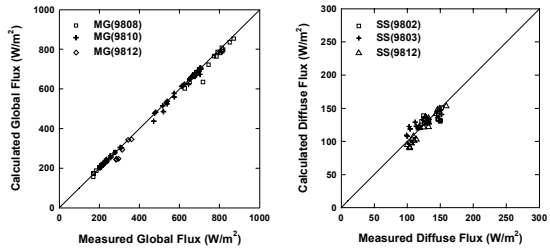

Fig. 2 (a): Scatter plots of downward surface solar flux between the simulated and measured global flux at Mandalgovi (left) and diffuse flux at Sri-Samrong (right) under the clear sky condition.

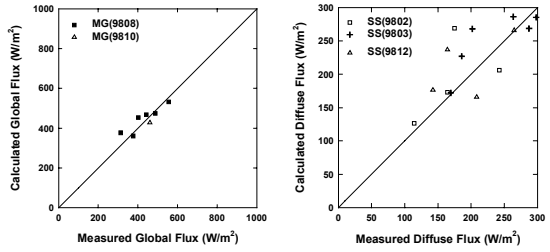

Fig. 2 (b): Same as in Fig. 2 (a) except the cloudy sky condition.

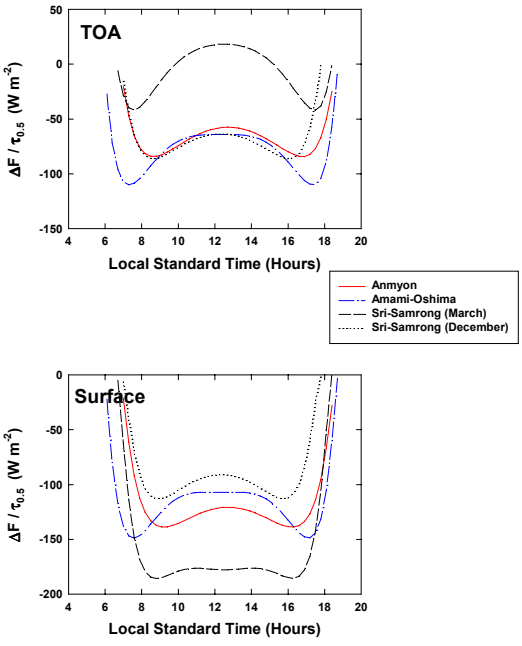

Fig. 3: The instantaneous aerosol radiative forcing at TOA and the surface on different aerosol optical properties as a function of local standard time.

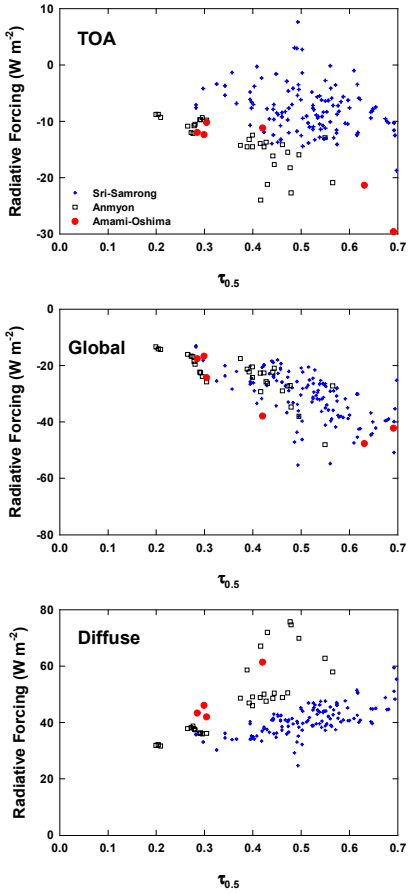

Fig. 4: 24-hour averaged aerosol radiative forcing with aerosol optical thickness at the wavelength of 0.5 μm at Anmyon (square), Sri-Samrong (crosshair), and Amami-Oshima (circle).